Electronic Supplementary Material (ESI) for Materials Chemistry Frontiers.

Morphology engineering induces the increase of FeP/CoP heterointerface density for efficient alkaline water splitting driven by the interfacial dual active sites

Yunmei Du[a], Lu Zhan [a], Yanru Liu[b], Ruixin Chen[a], Yunlei Fu[a], Bin Li*[c], and Lei Wang* [a,b]

[a] Shandong Engineering Research Center for Marine Environment Corrosion and Safety Protection, College of Environment and Safety Engineering, Qingdao University of Science and Technology, Qingdao 266042, P. R. China.

[b] College of Chemistry and Molecular Engineering, Qingdao University of Science and Technology, Key Laboratory of Eco-chemical Engineering, Key Laboratory of Optic-electric Sensing and Analytical Chemistry of Life Science, Taishan Scholar Advantage and Characteristic Discipline Team of Eco Chemical Process and Technology, Qingdao 266042, P. R. China.

[c] College of Materials Science and Engineering, Qingdao University of Science and Technology, Qingdao 266042, P. R. China.

*E-mail: binli@qust.edu.cn (Bin Li); inorchemwl@126.com (Lei Wang)

Experimental Section

1. Materials

Iron (III) chloride hexahydrate ($FeCl_3 \cdot 6H_2O$, 99%) were bought from Mackin, Shanghai. Iron (III) nitrate nonahydrate ($Fe(NO_3)_3 \cdot 9H_2O$, 98.5%) were bought by West Long Chemical Company, LTD. N, N-dimethylacetamide (DMA, 99%) were purchased from Beijing Chemical Company. N, N-dimethylformamide (DMF, 99%) were purchased from Alfa Aesar. 2-Aminoterephthalic acid (99%) were provided by Sigma-Aldrich. Cobalt (II) nitrate hexahydrate ($Co(NO_3)_2 \bullet 6H_2O$, 99%) were achieved from Innochem, Beijing. All the chemicals were used as received without further purification. Ultrapure water (Millipore Milli-Q grade) with a resistivity of 18.2 MΩ was used in all the experiments.

2. Electrochemical measurements

Electrochemical measurements toward HER, OER and Overall water splitting were performed by Gamry Instruments Reference 2000 electrochemical station with three-electrode system (including the Hg/Hg_2Cl_2 electrode, a graphite rod and the glassy carbon electrode (SCE) coated with the FeP/CoP catalysts). 20 μL of catalyst ink composed of 5 mg of the FeP/CoP catalysts and 1 mL of ethanol containing 5% nafion drop onto the surface of the clean SCE and electrochemical tests were performed after drying half minutes in 40 ℃ oven. In 1 M KOH, $E_{(RHE)} = E_{(SCE)} + 0.244\ V + 0.0592\ pH$. Generally, the electrochemical property and their conductivity toward HER as well as OER was directly recorded via linear sweep voltammetry (LSV) at 5 mV s^{-1} and Electrochemical Impedance Spectroscopy (EIS) with the frequency range of

0.1~100000 Hz, respectively. The long-time durability test of the FeP/CoP NMs was operated through using chronoamperometric (I-T curves) method at the constant potentials of -140 mV for HER and 1.54 V for OER. It is worth noting that for all LSV tests, iR correction is performed using the iR-compensation program that comes with the Gamry Instruments Reference 2000 electrochemical station. Electrochemical active surface area (ECSA) and the double-layer capacitance (C_{dl}) are obtained from the CV curves, and the ECSA value is proportional to the C_{dl} value. The calculation formula is ECSA= CDL/Cs= C_{dl}*S/Cs (S= 0.07065 cm^2, Cs=0.04 mF cm^{-2}).

3. Characterization

Qualitative analysis and crystal structure of the $FeCo_3P$ samples were implemented on X-ray powder diffraction (XRD) of X'Pert PRO MPD measurement with the scanning rate of 5 ° min^{-1}. The various morphology the FeP/CoP catalysts carries can be determined by SEM (JEOL, JSM-7500F). EDS data, TEM images as well as its related TEM mapping analysis were obtained by TEM (FEI, Tecnai-C20). Meanwhile, analysis of the electronic state of the external catalysts was gained by XPS test which was conducted on Thermo Scientific Escalab 250Xi.

4. DFT Calculation

All DFT calculations were performed as implemented in the Vienna Ab Initio Simulation Package (VASP). The projector augmented wave (PAW) method with the Perdew-Burke-Ernzerhof (PBE) was used to describe the interaction between the ions and the electrons with frozen-core approximation. A cut-off energy was set to 400 eV. Stationary points were

identified by the conjugate gradient method until the forces acting on each ion were smaller than 0.05 eV/Å. The convergence tolerance of the energy was set to be 10^{-4} eV. The k-points meshes of 1 × 1 ×1 was used for the Brillouim zone integration.

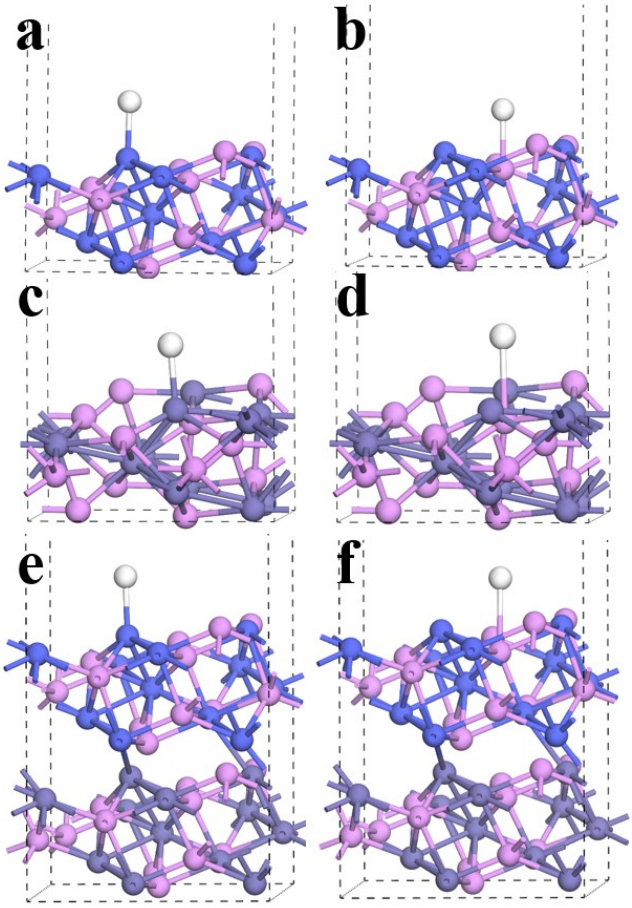

Fig. S1 Simulated (a-b) FeP, (c-d) CoP and (e-f) FeP/CoP models for formation of *H intermediates.

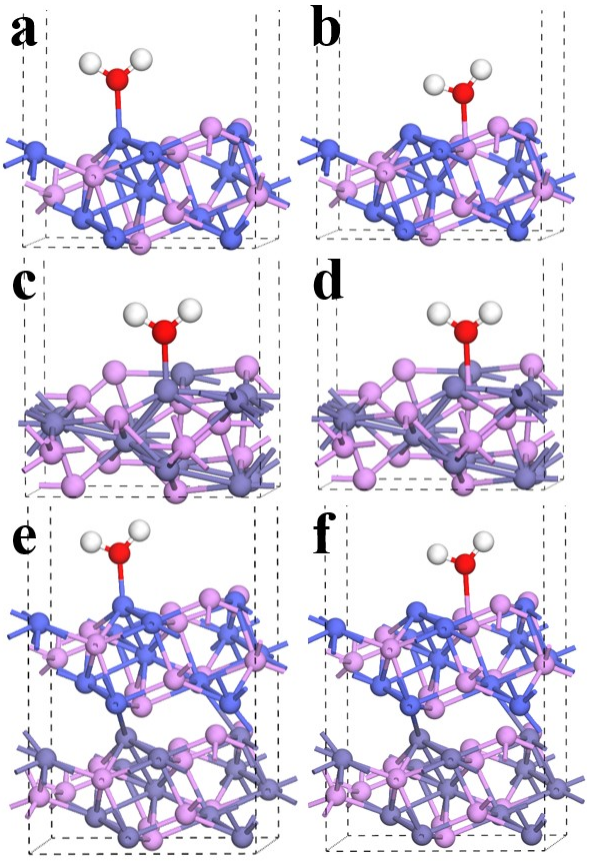

Fig. S2 Simulated (a-b) FeP, (c-d) CoP and (e-f) FeP/CoP models for adsorption of H_2O molecular.

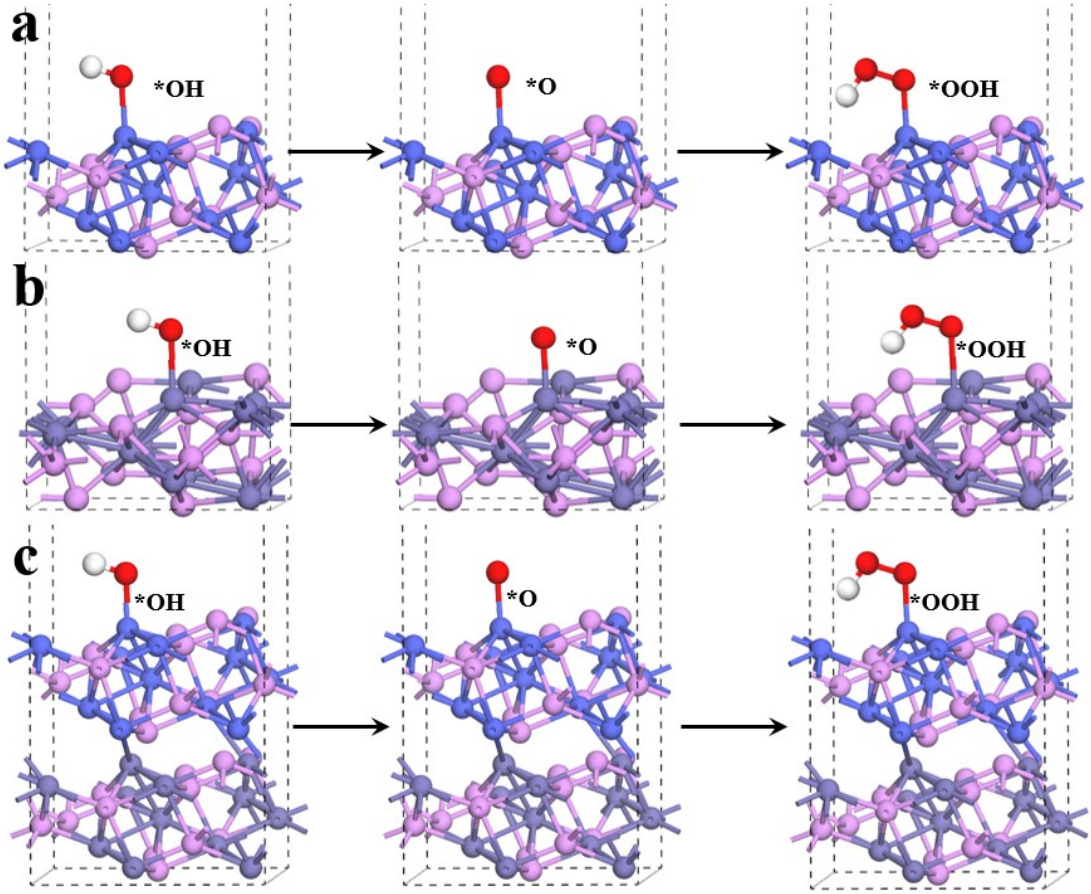

Fig. S3 Simulated (a-b) FeP, (c-d) CoP and (e-f) FeP/CoP models in the OER possess.

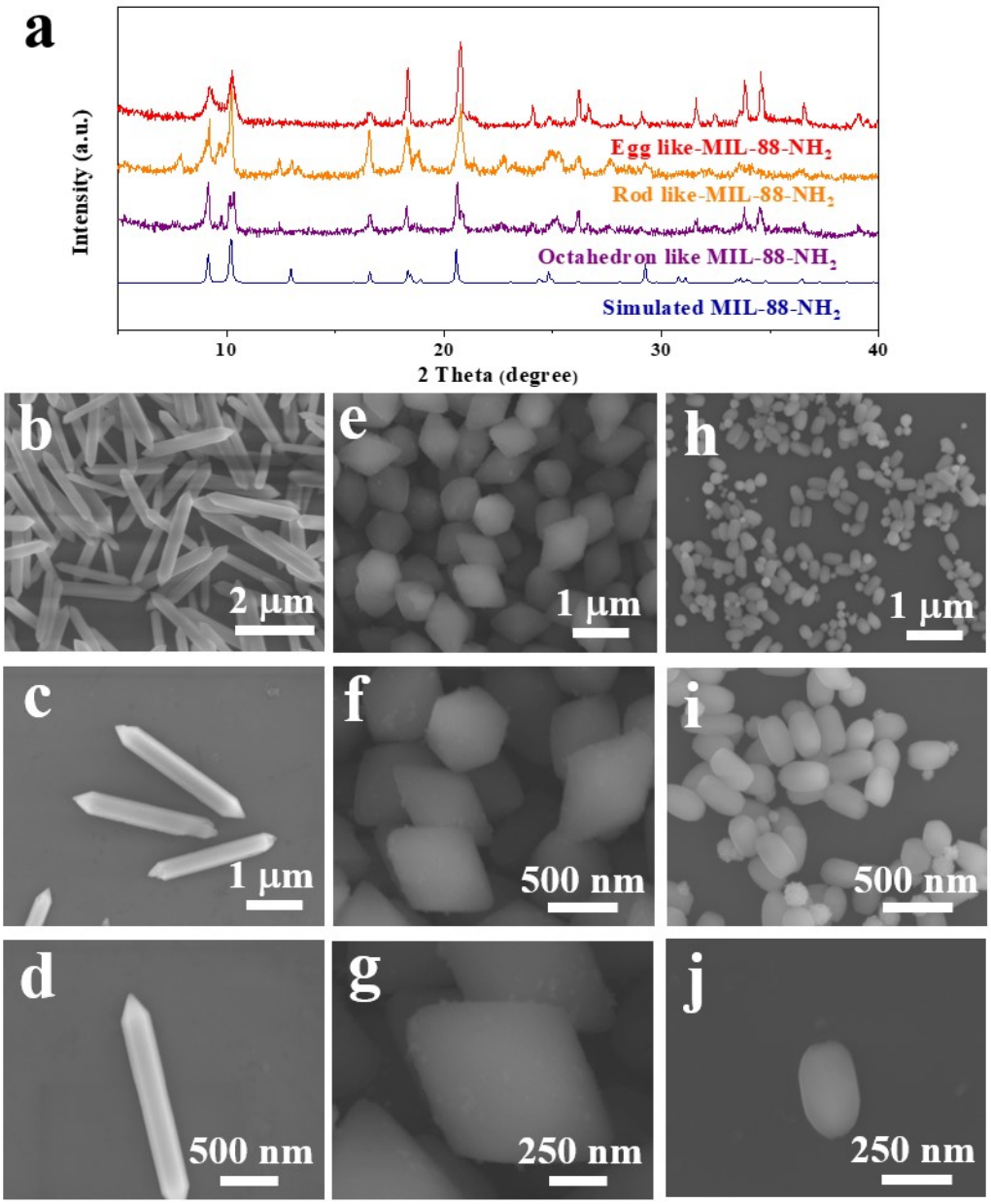

Fig. S4 (a) XRD pattern of the MIL-88-NH_2 with various morphologies (nano-egg, micro-rod, micro-octahedron); SEM images of the (b-d) micro-rod like-MIL-88-NH_2, (e-g) micro-octahedron like-MIL-88-NH_2, (h-j) nano-egg like-MIL-88-NH_2.

Table S1 ICP-OES results of the FeP/CoP catalysts with various sizes and morphologies

Catalysts	Fe/Co ratio in reagents	ICP Fe/Co ratio in MIL-88	ICP Fe/Co ratio in FeP/CoP
FeP/CoP NMs	1:1	1:1.06	1:1.01
FeP/CoP MOs	1:1	1:1.03	1:1.04
FeP/CoP MRs	1:1	1:0.99	1:1.02

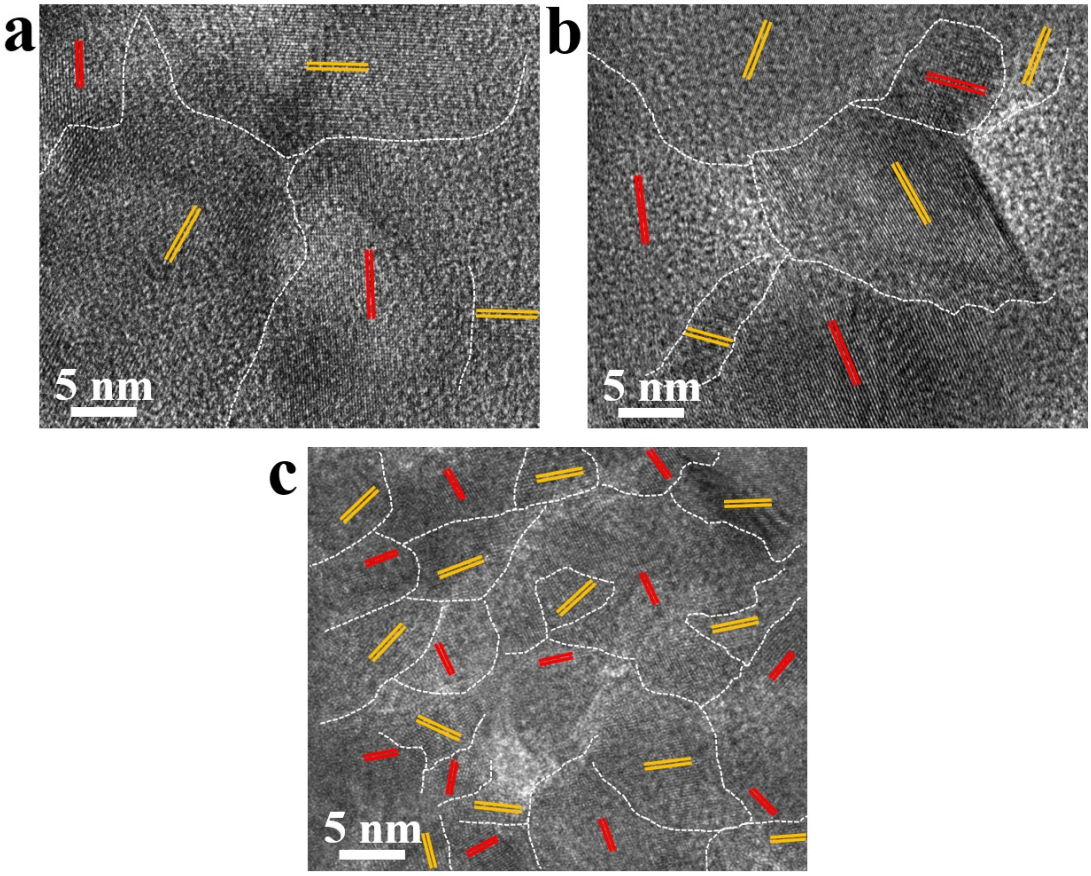

Fig. S5 HRTEM images of (a) FeP/CoP MRs, (b) FeP/CoP MOs, (c) FeP/CoP NMs. It is worth noting that the orange marked area represents the FeP phase, the red marked area represents the CoP phase and the white dashed line represents the heterogeneous interface.

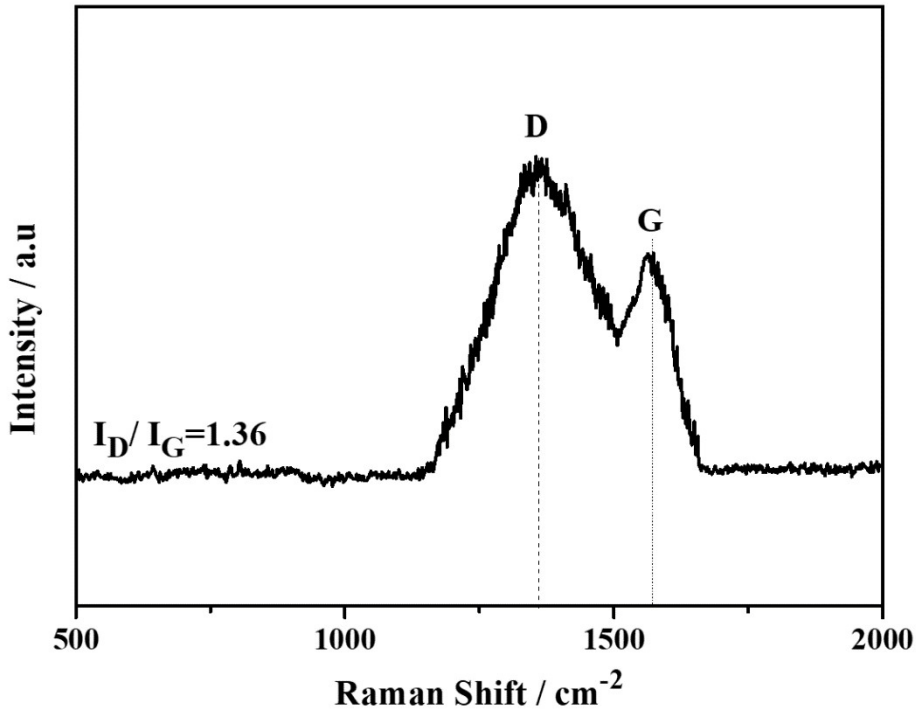

Fig. S6 Raman spectra of FeP/CoP NMs.

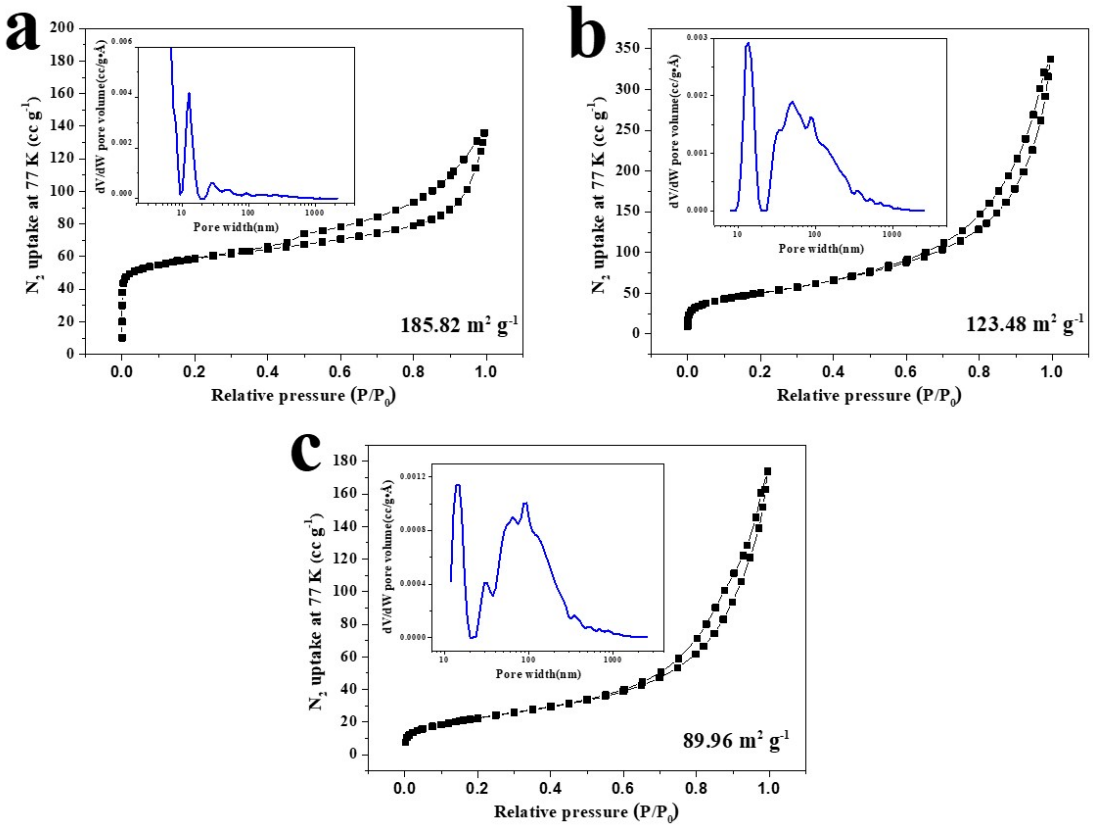

Fig. S7 N_2 adsorption-desorption isotherm (inset: corresponding NLDFT pore diameter distribution) of (a) the FeP/CoP NMs; (b) the FeP/CoP MOs; (c) the FeP/CoP MRs.

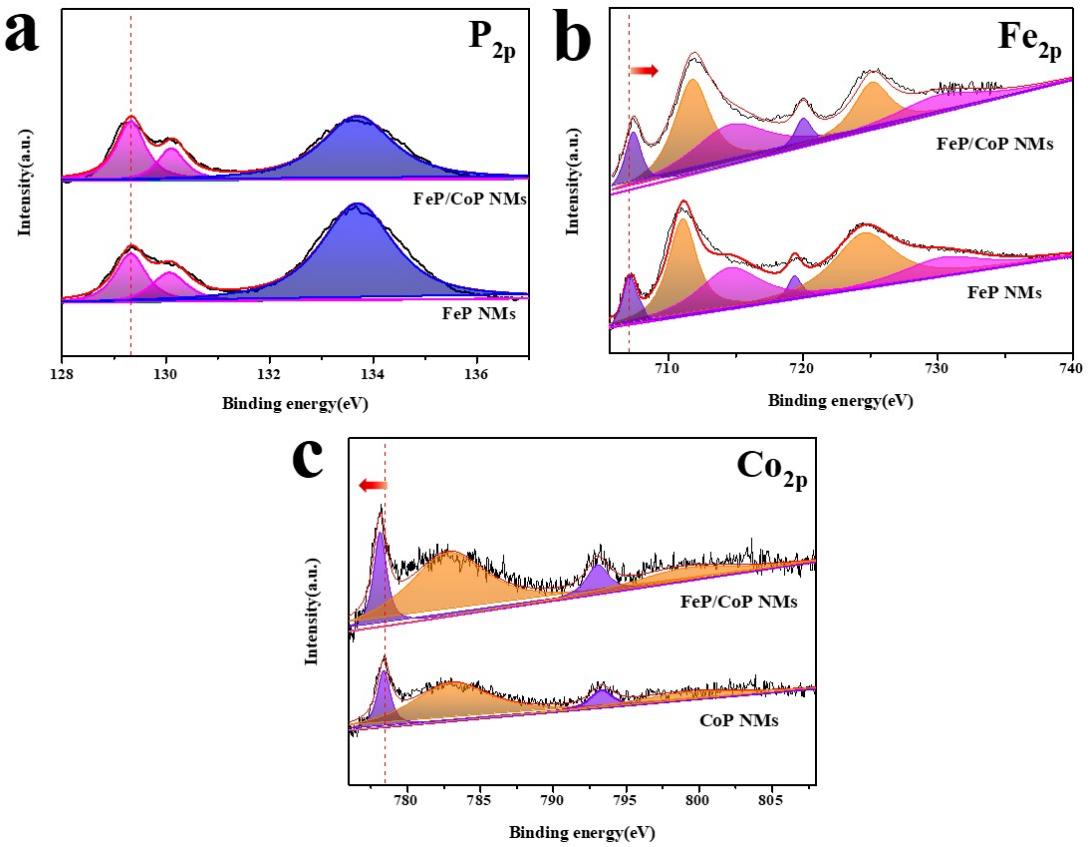

Fig. S8 XPS spectra of the FeP NMs, CoP NMs and FeP/CoP NMs: (a) P 2p, (b) Fe 2p, (c) Co 2p spectrum.

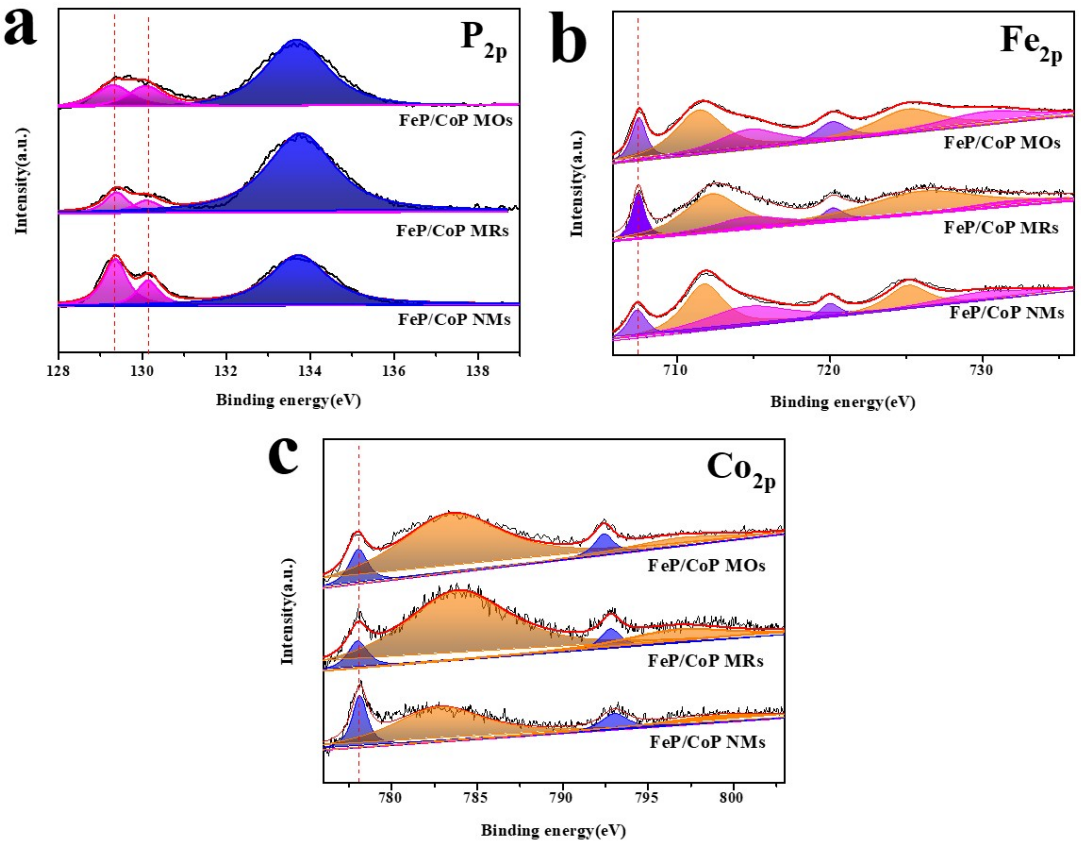

Fig. S9 XPS spectra of the FeP/CoP MRs, FeP/CoP MOs and FeP/CoP NMs: (a) P 2p, (b) Fe 2p, (c) Co 2p spectrum.

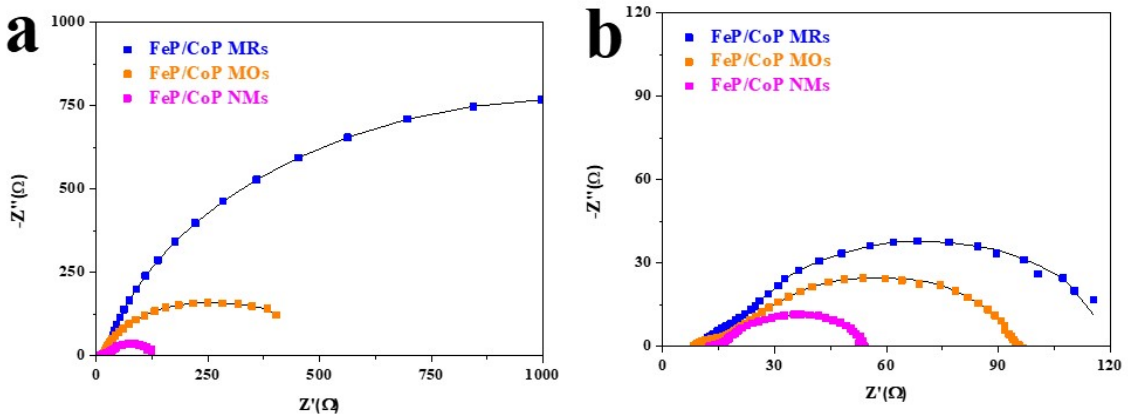

Fig. S10 (a) Nyquist plots at a specific voltage of -1.219 V for HER, (b) Nyquist plots at 0.5 V for OER.

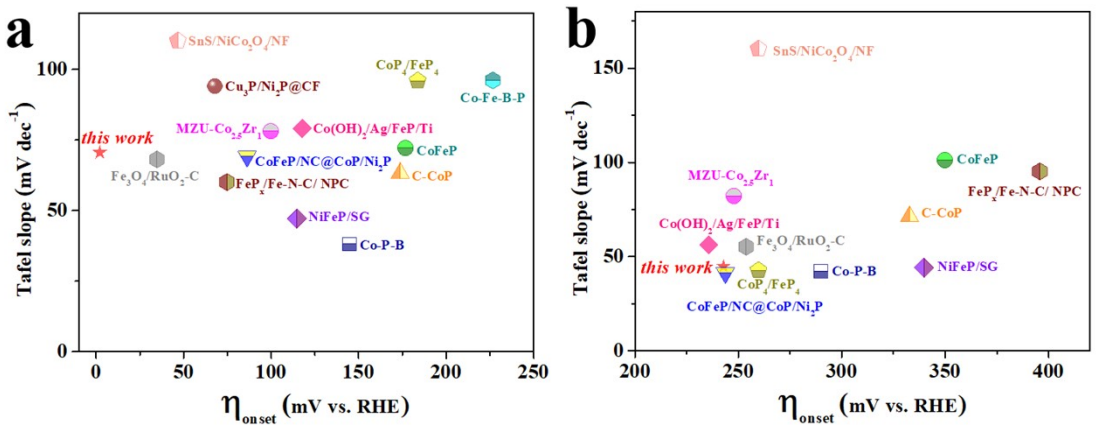

Fig. S11 Comparison of η_{onset} and Tafel plots for HER with the recently reported non-precious metal-based electrocatalysts, (d) Comparison of η_{onset} and Tafel plots for OER with the recently reported non-precious metal-based electrocatalysts.

Table S2 Electrocatalytic performances of other reported electrocatalysts in 1.0 M KOH electrolyte

Bifunctional electrocatalyst	HER		OER		Ref.
	η_{onset} (mV)	Tafel (mV dec^{-1})	η_{onset} (mV)	Tafel (mV dec^{-1})	
FeP/CoP NMS	2.4	70.4	243	44.5	This work
CoFeP	177	72	350	101	S1
FePx/Fe-N-C/ NPC	75	60	396	95	S2
NiFeP/SG	115	47	340	44	S3
C-CoP	174	63.1	333	71.1	S4
Co-Fe-B-P	227	96	225	40	S5
Co-P-B	145	38	290	42	S6
$Co(OH)_2$/Ag/ FeP/Ti	118	79	236	56	S7
SnS/$NiCo_2O_4$/N F	47	110	260	160	S8
CoFeP/NC@ CoP/Ni2P	86.5	69.0	244	41	S9
MZU-$Co_{2.5}Zr_1$	100	78	248	82	S10
Fe_3O_4/RuO_2-C	35	68	254	55	S11
CoP_4/FeP_4	184	95.9	260	42.4	S12
Cu_3P/Ni_2P@CF	68	94		72	S13

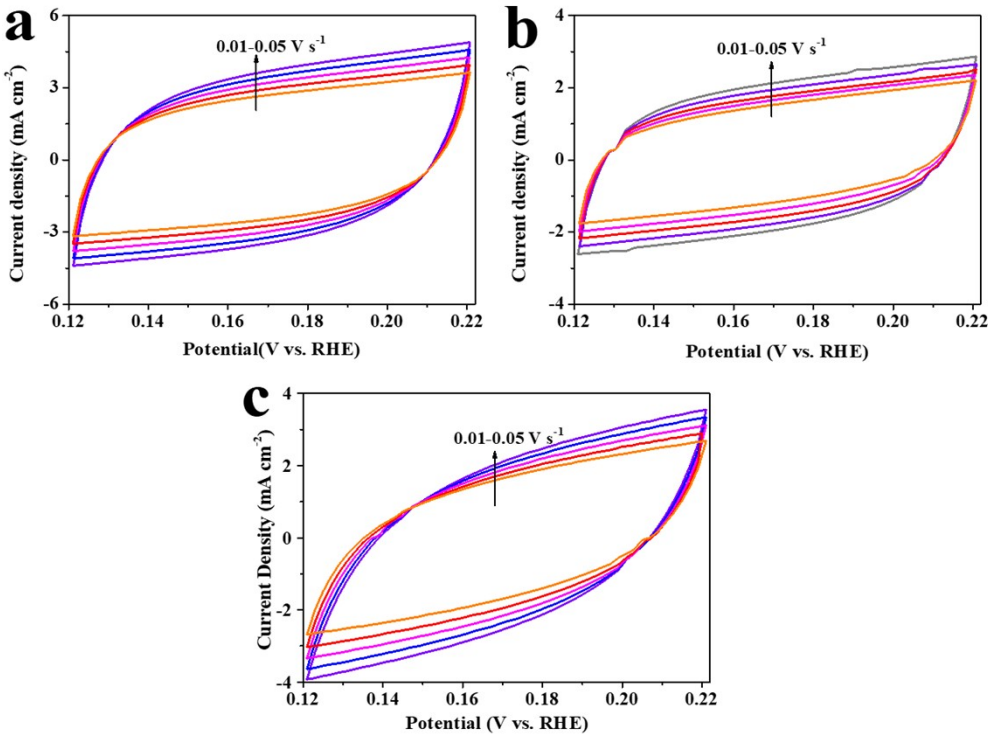

Fig. S12 CV curves of the (a) FeP/CoP NMs, (b) FeP/CoP MRs and (c) FeP/CoP MOs.

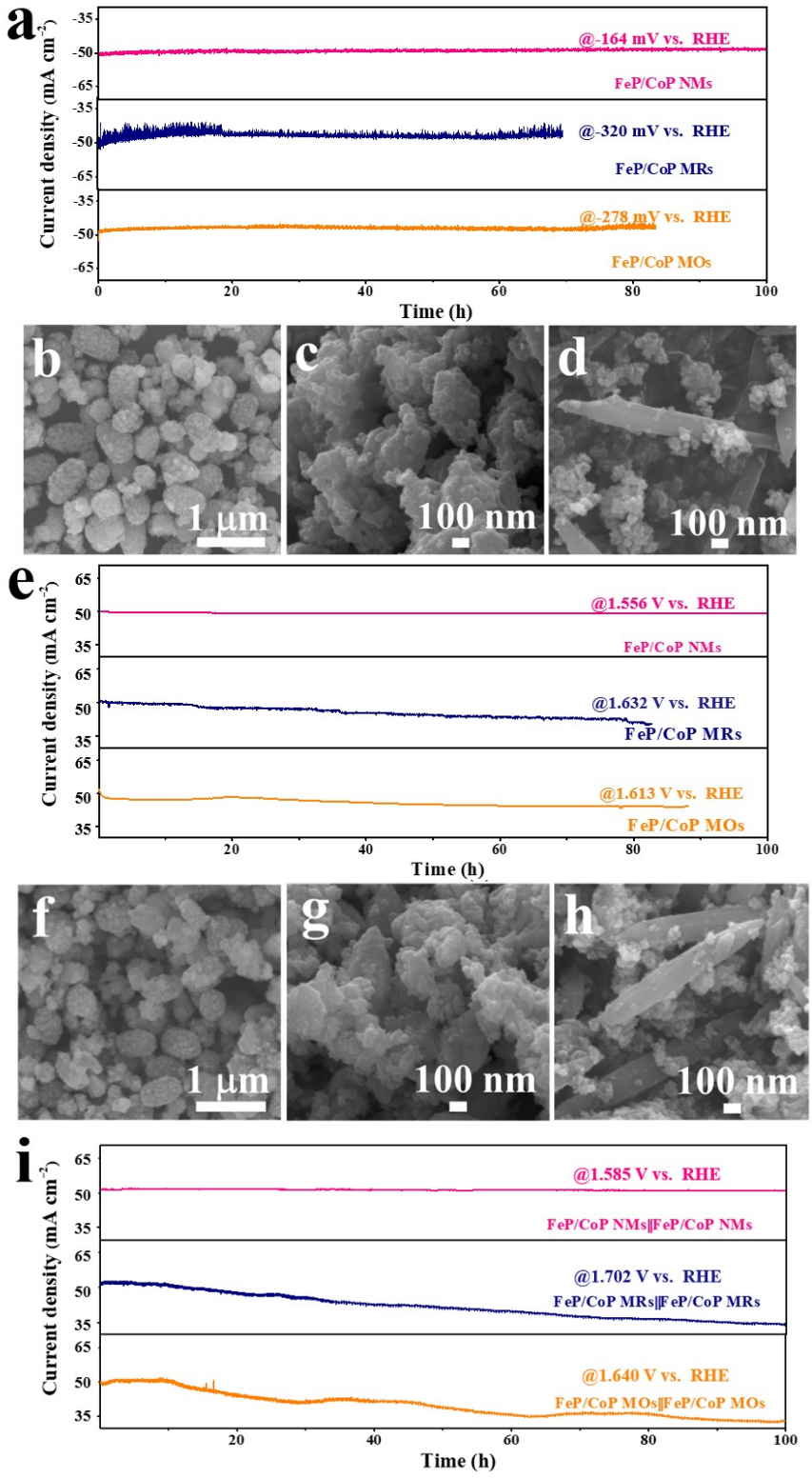

Fig. S13 (a) The I-T curves of the FeP/Co P NMs, FeP/CoP MOs and the FeP/CoP MRs for HER at the static voltage of -164, -278, -320 mV, respectively; Post-HER SEM images of (b) the FeP/CoP NMs, (c) the FeP/CoP Mos, (d) the FeP/CoP MRs; (e)

The I-T curves of the FeP/CoP NMs, FeP/CoP MOs and the FeP/CoP MRs for OER at the static voltage of 1.556, 1.613, 1.632 V, respectively; Post-OER SEM images of (f) the FeP/CoP NMs, (g) the FeP/CoP MOs, (h) the FeP/CoP MRs; (i) The I-T curve of the FeP/CoP NMs||FeP/CoP NMs, FeP/CoP MOs|| FeP/CoP MOs and the FeP/CoP MRs|| FeP/CoP MRs for water splitting at the cell voltage of 1.585 V, 1.640, 1.702 V, respectively.

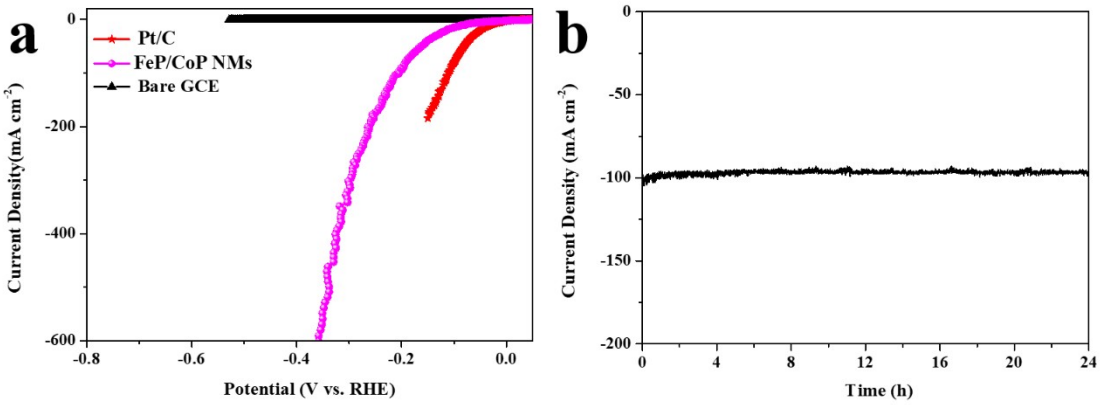

Fig. S14 (a) HER polarization curves of the FeP/CoP NMs and (b) the I-T curves of the FeP/CoP NMs for HER at the static voltage of - 212 mV.

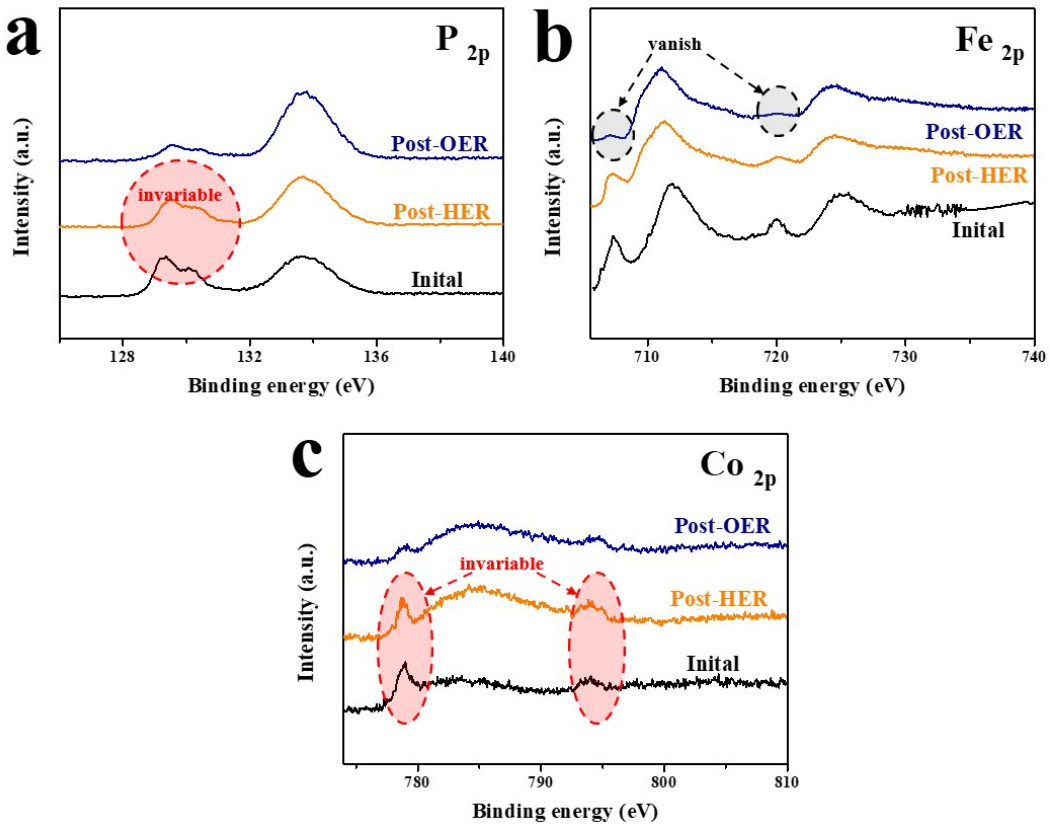

Fig. S15 XPS spectra of the FeP/CoP NMs after stability test toward HER and OER in alkaline electrolyte solution: (a) P 2p; (b) Fe 2p; (c) Co 2p.

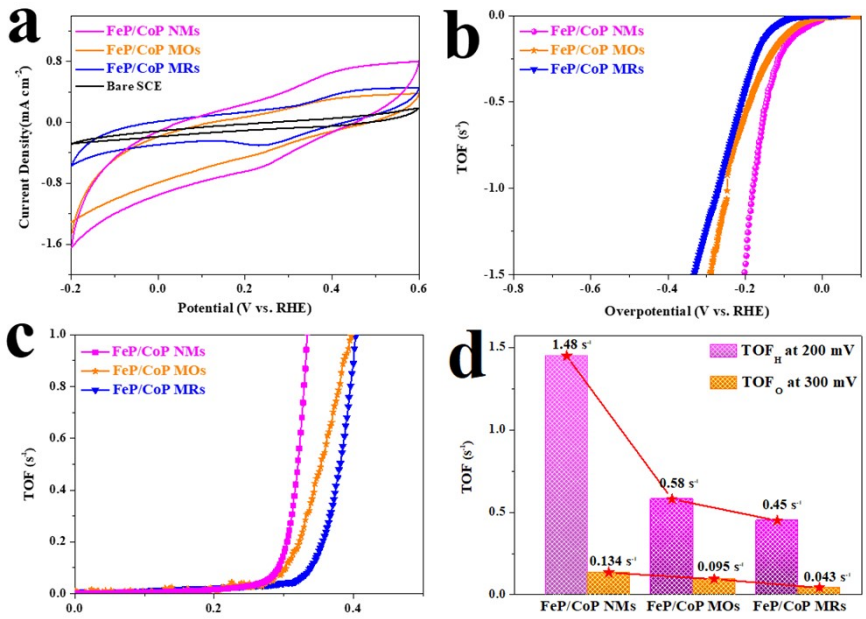

Fig. S16 (a) Cyclic Voltammograms of FeP/CoP NMs, FeP/CoP MOs, FeP/CoP MRs in 1.0 M PBS at a scan rate of 100 mV s^{-1}, (b) the TOFs of the as-prepared catalysts at different potentials in 1.0 M KOH for HER, (c) the TOFs at different potentials in 1.0 M KOH for OER, (d) TOFH of the obtained catalysts at an overpotential of 200 mV vs. RHE and TOFO at 300 mV vs. RHE.

Table S3 ICP-OES results of the FeP/CoP NMs and FeP/CoP NMs-n (n=2.0, 0.5) catalysts

Catalysts	Fe/Co ratio in reagents	ICP Fe/Co ratio in MIL-88	ICP Fe/Co ratio in FeP/CoP product
FeP/CoP NMs-0.5	2:1	2.03:1	1.99:1
FeP/CoP NMs	1:1	1:1.06	1:1.01
FeP/CoP NMs-2.0	1:2	1:1.98	1:2.01

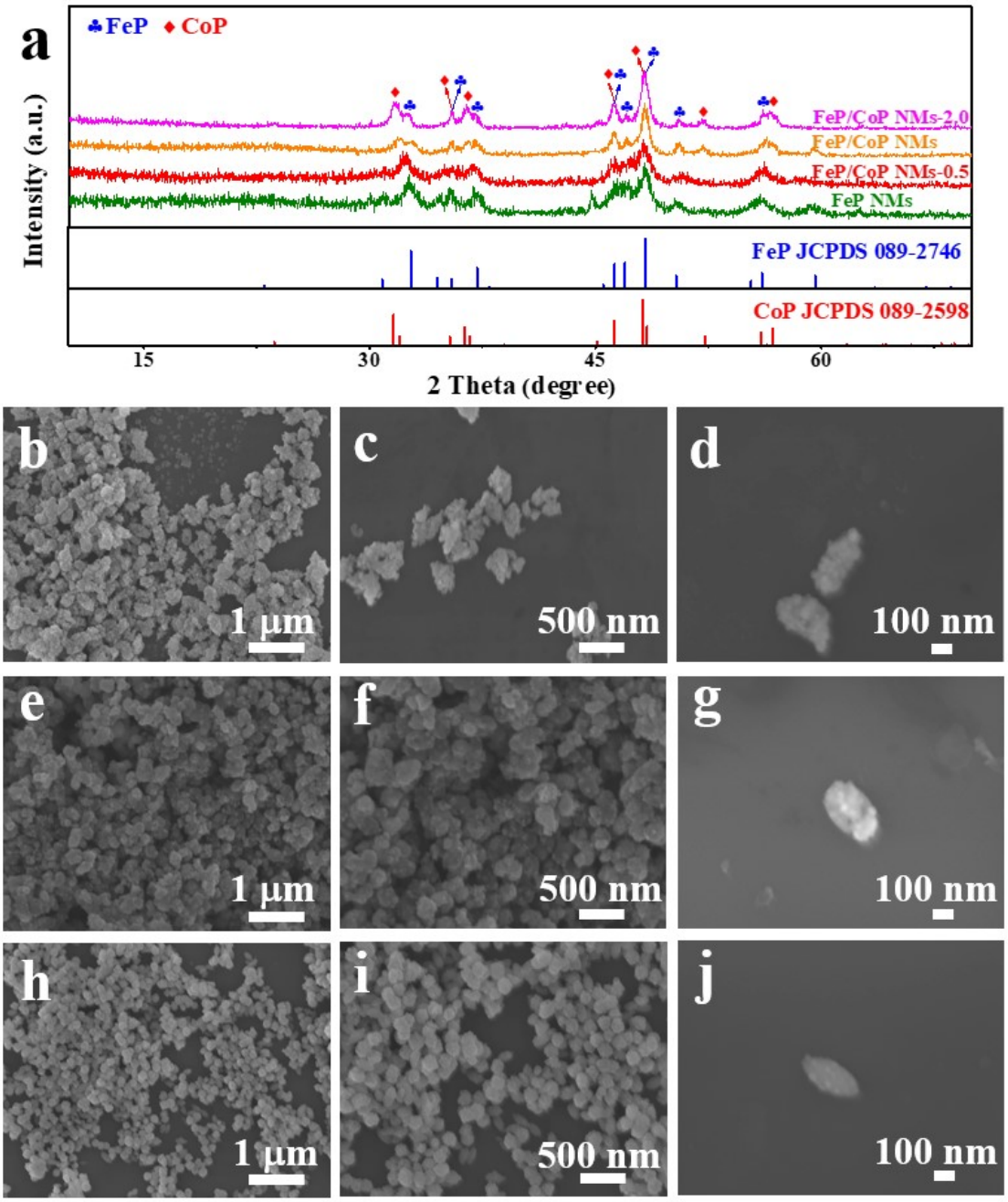

Fig. S13 (a) XRD of FeP NMs, FeP/CoP NMs and FeP/CoP NMs-n catalysts (n=2.0, 0.5), SEM images of the (b-d) the FeP NMs, (e-g) the FeP/CoP NMs-2.0 and (h-j) the FeP/CoP NMs-0.5.

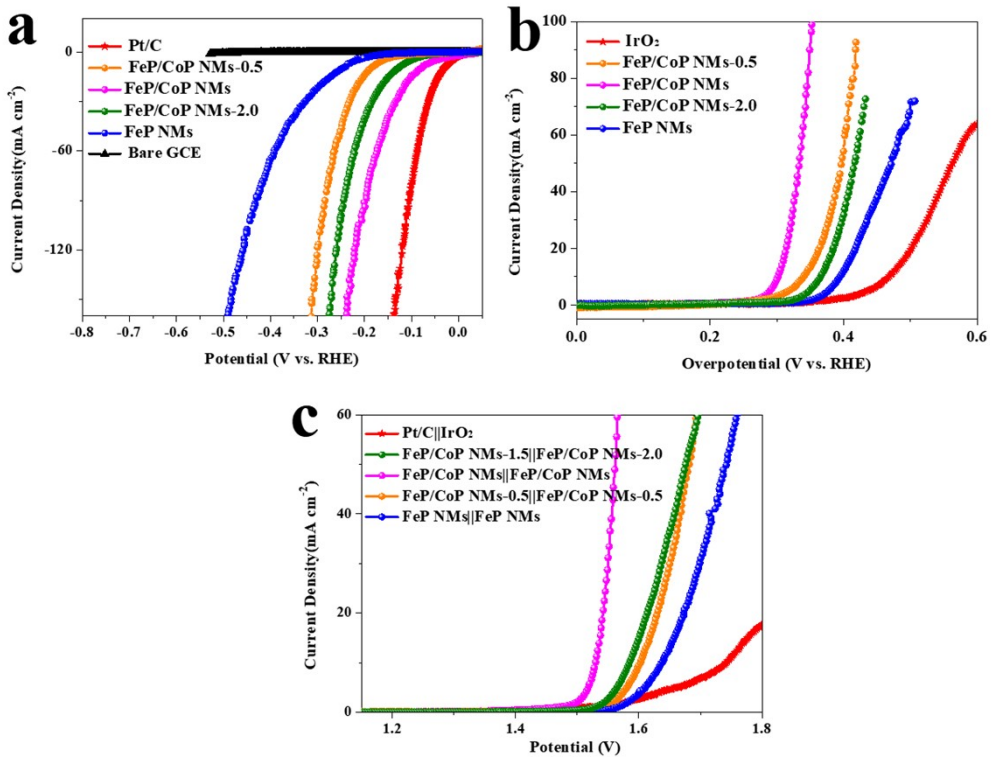

Fig. S18 Electrochemical performances of Pt/C, IrO_2, FeP NMs, FeP/CoP NMs and FeP/CoP NMs-n (n=2.0, 0.5) catalysts: (a) HER polarization curves; (b) OER polarization curves; (c) Overall water splitting polarization curves.

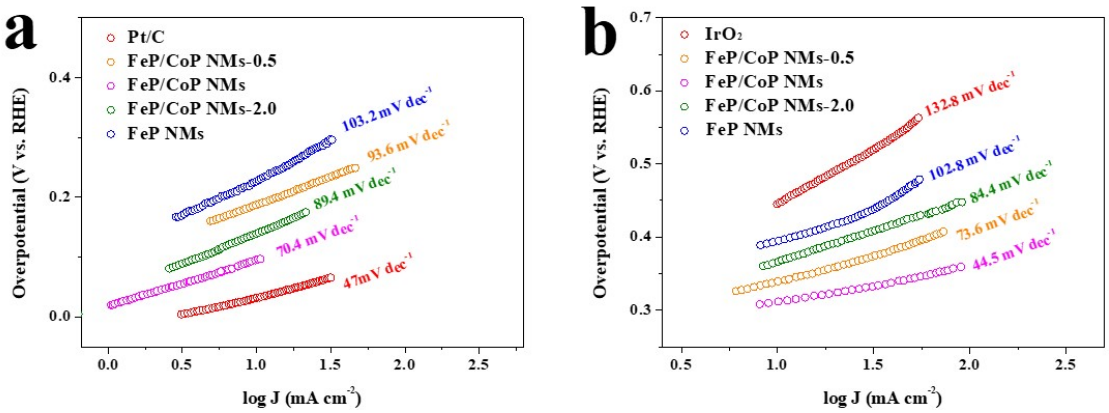

Fig. S19 The corresponding Tafel plots of Pt/C, FeP NMs, FeP/CoP NMs and FeP/CoP NMs-n (n=2.0, 0.5) catalysts toward (a) HER and (b) OER.

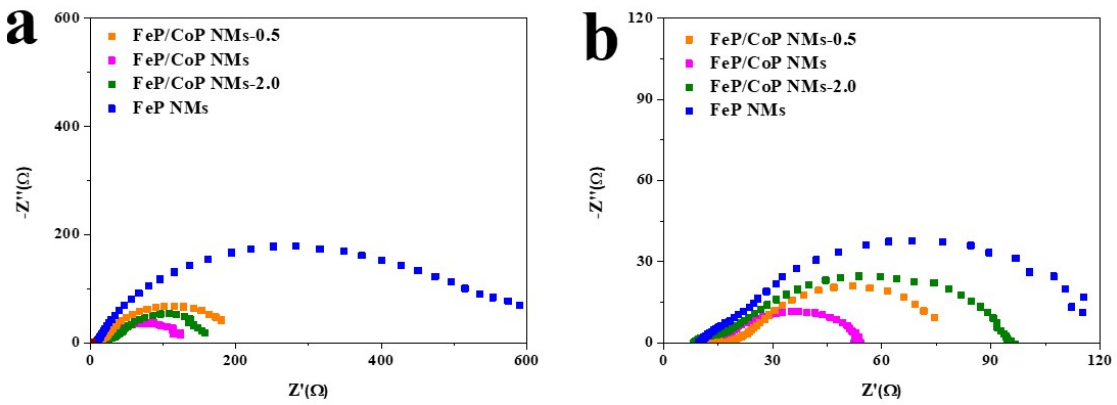

Fig. S20 The Nyquist plots of the FeP NMs, FeP/CoP NMs and FeP/CoP NMs-n (n=2.0, 0.5) catalysts toward (a) HER at 150 mV, (b) OER at 0.5 V.

[S1] Y. Du, H. Q. Qu, Y. R. Liu, Y. Han, L. Wang, B. Dong, Bimetallic CoFeP hollow microspheres as highly efficient bifunctional electrocatalysts for overall water splitting in alkaline media, Appl. Surf. Sci., 2019, 465,816-823.

[S2] Q. Qin, H. Jang, P. Li, B. Yuan, X. Liu, J. Cho, A Tannic Acid-Derived N-, P-Codoped Carbon-Supported Iron-Based Nanocomposite as an Advanced Trifunctional Electrocatalyst for the Overall Water Splitting Cells and Zinc-Air Batteries, Adv. Energy Mater., 2019, 9, 1803312.

[S3] R. Q. Li, B. L. Wang, T. Gao R. Zhang, C. Xu, X. Jiang, J. Zeng, Y. Bando, P. Hu, Y. Li, X. B. Wang, Monolithic electrode integrated of ultrathin NiFeP on 3D strutted graphene for bifunctionally efficient overall water splitting, Nano Energy, 2019, 58, 870-876.

[S4] W. Li, G. Cheng, M. Sun, Z. Wu, G. L. Liu, D. Su, B. Lan, S. X. Mai, L. Chen and L. Yu, C-CoP hollow microporous nanocages based on the phosphating regulation: a high-performance bifunctional electrocatalyst for overall water splitting, Nanoscale, 2019, 11, 17084-17092.

[S5] Z. Wu, D. Nie, M. Song, T. Jiao, G. Fu and X. Liu, Facile Synthesis of Co-Fe-B-P Nanochains as Efficient Bifunctional Electrocatalysts for Overall Water-splitting, Nanoscale, 2019, 11, 7506-7512.

[S6] A. Chunduri, S. Gupta, O. Bapat, A. Bhide, R. Fernandes, M.K. Patel, V. Bambole, A. Miotello and N. Patel, A unique amorphous cobalt-phosphide-boride bifunctional electrocatalyst for enhanced alkaline water-splitting, Appl. Catal. B-Environ., 2019, 259, 118051.

[S7] X. Ding, Y. Xia, Q. Li, S. Dong, X. Jiao and D. Chen, Interface Engineering of $Co(OH)_2$/Ag/FeP Hierarchical Superstructure as Efficient and Robust Electrocatalyst for Overall Water Splitting, ACS Appl. Mater. Inter., 2019, 11, 7936-7945.

[S8] G. John, S. Gopalakrishnan, A. Sharan, et al, Exploring the Heterostructure Engineering of SnS/$NiCo_2O_4$ for Overall Water Splitting, Energy Fuels, 2023, 37, 624–634.

[S9] R. Fu, Q. Jiao, C. Yang, et al, CoFeP/NC@CoP/Ni_2P heterostructure for efficient overall water splitting, New J. Chem., 2023,47, 1226-1233.

[S10] P. Chen, M. Wang, G. Li, et al, Construction of ZIF-67-On-UiO-66 Catalysts as a Platform for Efficient Overall Water Splitting, Inorg. Chem., 2022, 61, 18424–18433.

[S11] A. Shekhawat, R. Samanta, S. Barman, MOF-Derived Porous Fe_3O_4/RuO_2-C Composite for Efficient Alkaline Overall Water Splitting, ACS Appl. Energy Mater., 2022, 5, 6059–6069.

[S12] H. Yan, X. Xiao, X. Liu, et al, Designing of CoP_4/FeP_4 with hollow nanocages as bifunctional catalysts for overall water splitting, Int. J. Hydrog. Energy, 2022, 47, 23230-23239.

[S13] H. Liu, J. Gao, X. Xu, et al, Oriented construction Cu_3P and Ni_2P heterojunction to boost overall water splitting, Chem. Eng. J., 2022, 448, 137706.